2-16-2016

Determination of the Goos-Hänchen Shift in Dielectric WaveGuides via Photo Emission Electron Microscopy in the Visible Spectrum

Theodore Stedmark
Portland State University, stenmark@pdx.edu

Robert Campbell Word
Portland State University, wordr@pdx.edu

Rolf Könenkamp
Portland State University, rkoe@pdx.edu

Citation Details

Stenmark, T., Word, R. C., & Könenkamp, R. (2016). Determination of the Goos-Hänchen shift in dielectric waveguides via photo emission electron microscopy in the visible spectrum. Optics Express, 24(4), 3839–48.

Determination of the Goos-Hänchen shift in dielectric waveguides via photo emission electron microscopy in the visible spectrum

Theodore Stenmark,* R. C. Word, and R. Könenkamp

Department of Physics, Portland State University, Portland, Oregon, 97207, USA
**stenmark@pdx.edu*

Abstract: Photoemission Electron Microscopy (PEEM) is a versatile tool that relies on the photoelectric effect to produce high-resolution images. Pulse lasers allow for multi-photon PEEM where multiple photons are required excite a single electron. This non-linear process can directly image the near field region of electromagnetic fields in materials. We use this ability here to analyze wave propagation in a linear dielectric waveguide with wavelengths of 410nm and 780nm. The propagation constant of the waveguide can be extracted from the interference pattern created by the coupled and incident light and shows distinct polarization dependence. The electromagnetic field interaction at the boundaries can then be deduced which is essential to understand power flow in wave guiding structures. These results match well with simulations using finite element techniques.

OCIS codes: (180.0180) Microscopy; (240.0240) Optics at surfaces; (070.0070) Fourier optics and signal processing; (070.7345) Wave propagation.

References and links

1. R. Könenkamp, R. C. Word, G. F. Rempfer, T. Dixon, L. Almaraz, and T. Jones, "5.4 nm spatial resolution in biological photoemission electron microscopy," Ultramicroscopy **110**(7), 899–902 (2010).
2. L. Zhang, A. Kubo, L. Wang, H. Petek, and T. Seideman, "Imaging of surface plasmon polariton fields excited at a nanometer-scale slit," Phys. Rev. B **84**(24), 245442 (2011).
3. C. Lemke, T. Leißner, S. Jauernik, A. Klick, J. Fiutowski, J. Kjelstrup-Hansen, H. G. Rubahn, and M. Bauer, "Mapping surface plasmon polariton propagation via counter-propagating light pulses," Opt. Express **20**(12), 12877–12884 (2012).
4. J. P. S. Fitzgerald, R. C. Word, and R. Könenkamp, "Subwavelength visualization of light in thin film waveguides with photoelectrons," Phys. Rev. B **89**(19), 195129 (2014).
5. J. P. S. Fitzgerald, R. C. Word, S. D. Saliba, and R. Könenkamp, "Photonic near-field imaging in multiphoton photoemission electron microscopy," Phys. Rev. B **87**(20), 205419 (2013).
6. P. K. Tien, "Integrated optics and new wave phenomena in optical waveguides," Rev. Mod. Phys. **49**(2), 361–420 (1977).
7. F. Goos and H. Hänchen, "Ein neuer und fundamentaler Versuch zur Totalreflexion," Ann. Phys. **6**(7), 333–346 (1947).
8. T. A. F. König, P. A. Ledin, J. Kerszulis, M. A. Mahmoud, M. A. El-Sayed, J. R. Reynolds, and V. V. Tsukruk, "Electrically tunable plasmonic behavior of nanocube-polymer nanomaterials induced by a redox-active electrochromic polymer," ACS Nano **8**(6), 6182–6192 (2014).
9. H. Kim, G. Horwitz, G. Kushto, A. Piqué, Z. H. Kafafi, C. M. Gilmore, and D. B. Chrisey, "Effect of film thickness on the properties of indium tin oxide thin films," J. Appl. Phys. **88**(10), 6021–6025 (2000).
10. R. Schlaf, H. Murata, and Z. H. Kafafi, "Work function measurements on indium tin oxide films," J. Electron Spectrosc. Relat. Phenom. **120**(1–3), 149–154 (2001).
11. A. Yariv, *Optical Electronics* (Saunders College Publishing, 1991).
12. J. J. Burke, Opt. Sci. Newsletter (U. Ariz.) **5**, 66 (1971).
13. C. R. Pollock, M. Lipson, *Integrated Photonics* (Springer-Verlag 2003). Appendix A pp. (363–365)
14. X. Liu, Z. Cao, P. Zhu, and Q. Shen, "Solution to causality paradox upon total reflection in optical planar waveguide," Phys. Rev. E Stat. Nonlin. Soft Matter Phys. **73**(1), 016615 (2006).
15. A. Gedeon, "Effective thickness of optical waveguides in tunable couplers," J. Opt. Soc. Am. **64**(5), 615–618 (1974).
16. V. Ramaswamy, "Ray model of energy and power flow in anisotropic film waveguides," J. Opt. Soc. Am. **64**(10), 1313–1320 (1974).
17. I. Newton, *Opticks* (Dover, 1952).
18. K. Artmann, "Berechnung der Seitenversetzung des totalreflektierten Strahles," Ann. Phys. **6**(2), 87–102 (1948).

#255587 Received 14 Dec 2015; revised 12 Jan 2016; accepted 13 Jan 2016; published 16 Feb 2016

19. R. H. Renard, "Total reflection: a new evaluation of the Goos–Hänchen Shift," J. Opt. Soc. Am. **54**(10), 1190–1197 (1964).
20. B. R. Horowitz and T. Tamir, "Lateral displacement of a light beam at a dielectric interface," J. Opt. Soc. Am. **61**(5), 586–592 (1971).
21. K. W. Chiu and J. J. Quinn, "On the Goos-Hanchen Effect: a simple example of time delay scattering process," Am. J. Phys. **40**(12), 1847–1851 (1972).
22. H. Kogelnik, *Theory of Optical Waveguides in Guided-Wave Optoelectronics*, T. Tamir, ed. (Springer-Verlag, 1988).
23. H. Kogelnik and H. P. Weber, "Rays, stored energy and power flow in dielectric waveguides," J. Opt. Soc. Am. **64**(2), 174–185 (1974).
24. P. K. Tien, "Light waves in thin films and integrated optics," Appl. Opt. **10**(11), 2395–2413 (1971).
25. P. T. Leung, C. W. Chen, and H. P. Chiang, "Large negative Goos-Hanchen shift at metal surfaces," Opt. Commun. **276**(2), 206–208 (2007).
26. R. Yang, W. Zhu, and J. Li, "Realization of "trapped rainbow" in 1D slab waveguide with surface dispersion engineering," Opt. Express **23**(5), 6326–6335 (2015).
27. K. L. Tsakmakidis, A. D. Boardman, and O. Hess, "'Trapped rainbow' storage of light in metamaterials," Nature **450**(7168), 397–401 (2007).
28. D. H. Foster, A. K. Cook, and J. U. Nöckel, "Goos-Hänchen induced vector eigenmodes in a dome cavity," Opt. Lett. **32**(12), 1764–1766 (2007).

1. Introduction

Photoemission Electron Microscopy (PEEM) is a powerful imaging technique for observing electromagnetic near-field phenomena on the nanoscale. By directing a pulsed laser beam onto a sample incident photons excite electron emission via the photoelectric effect. The photoelectrons are used to produce high quality images down to 5nm resolution [1]. The contrast of the image is dependent on the spatial electron yield, which depends on the work function, surface electron density, and topography of the material as well as the energy and intensity of the incident photons. Traditional PEEM employs ultraviolet or x-ray sources, which are convenient due to the high energy only requiring one photon to overcome the work function of many materials.

Multiphoton PEEM is a method in which the work function of the material and the energy of the photons are such that multiple photons are required to generate electron emission. This method has recently been used for the study of surface plasmon polaritons [2,3] as the non-linear excitation process allows for observing localized electromagnetic fields in the visible and infrared region. These have attracted considerable attention as plasmonics provides a way to confine light past the diffraction limit. PEEM has extensive potential for this application as it provides direct imaging of the optical near-field, is non-invasive and is not subject to light optical diffraction limit but rather is limited by the electron optics of the microscope.

In addition to studying surface plasmon polaritions, the multiphoton process is also well-suited for observing electromagnetic fields on the surface of photonic structures [4]. In the past years we have used this method to characterize optical wave propagation in nanostructured optical waveguides [5]. PEEM is ideal for the study of surface phenomena because photoelectrons and the information they carry originate from the upper ~10 nm of the sample.

In this paper we examine a dielectric wave guide in the visible and near infrared regime. Waveguide structures are among the cornerstones of optical devices for communications and computing and are used in combination with antennas, sensors and other types of integrated optical devices [6]. Because dielectric waveguides select discrete modes of propagation, we are able to use the interference of an incident beam with the propagating light in the waveguide, as depicted in Fig. 1, to fully characterize the dielectric slab waveguide structures. The interference creates strong variation in electromagnetic fields which PEEM is highly sensitive to due to the non-linearity of multiphoton excitation.

The high, sub-wavelength resolution of PEEM not only allows for wave propagation analysis but also provides insight to fundamental aspects of light propagation in dielectrics. In this paper we demonstrate this capability by experimentally determining a polarization dependent shift of the light propagation path upon total internal reflection. In a dielectric waveguide the total internal reflection does not fully contain the electromagnetic field in the core of the waveguide, rather the electric field bleeds into the surrounding materials in an

#255587 Received 14 Dec 2015; revised 12 Jan 2016; accepted 13 Jan 2016; published 16 Feb 2016

evanescently decaying wave. This is the root of a phenomenon known as the Goos-Hänchen shift [7], which is a lateral shift of a finite beam due to the dependence of the evanescent field on incident angle of the beam. The magnitude of the Goos-Hänchen shift affects the allowed modes of propagation and thus also affects the details of the stationary interference pattern observed in PEEM.

We show that the existence and magnitude of the Goos-Hänchen shift can directly be inferred from PEEM images. We are also able to determine the polarization dependence of the Goos-Hänchen shift. Here we present results at optical wavelengths of $\lambda = 410$ and 780 nm to demonstrate that PEEM can be applied with high precision across the complete visible range, even to the near infrared region.

2. Experimental methods

The sample consisted of a 0.2 mm borosilicate glass sheet coated with an indium-tin-oxide (ITO) layer of ~290 ± 20 nm thickness acquired from SPI supplies, Inc. The refractive index of ITO is 2.14 ± 0.01 at a wavelength $\lambda = 410$ nm and n = 1.78 ± 001 at $\lambda = 780$ nm [8]. Other optical properties of ITO thin films such as absorption are dependent on the thickness of the film [9]. The real part of the refractive index of the glass substrate is 1.53 ± . 01.

Parallel strip waveguides were defined with a FEI Strata 273 focused ion beam (FIB). A deep narrow groove was milled to a depth of 240nm into the sample with dimensions of 6.0 µm x 0.4 µm at the beginning of the waveguides. This allowed for in-coupling of light into the waveguide through diffraction. A thinned waveguide region was milled to a depth of ~40 nm ± 10 nm and dimensions of 2.0µm × 5.0µm connecting to the center portion of the groove as indicated in Fig. 1. This waveguide was imaged by PEEM at $\lambda = 410$ nm and $\lambda = 780$ nm.

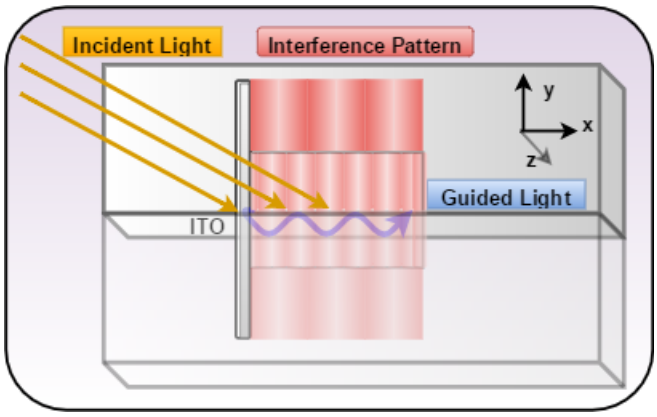

Fig. 1. Basic waveguide experiment: polarized light is directed towards the milled slit at an incident angle of 60°. Interference between the wave-guided light and the non-scattered incident light generates an interference pattern as indicated

As shown in Fig. 1, the sample was oriented in the PEEM such that the groove was perpendicular to the incident laser light. The optical excitation beam was incident at an angle of 60° from the sample normal. In this configuration light is coupled into the groove of the waveguide and propagates laterally in the waveguide. This guided light interferes with the direct excitation light and generates a stationary interference pattern. This pattern is imaged in the PEEM with a spatial resolution of ~30 nm and can be analyzed in terms of the propagation constants of the wave-guided light.

The Spectra-Physics Mai Tai Ti:Sapphire laser used in the experiment generates 80-fs pulses with energies in the low nJ range at a rate of 80 MHz. A Del Mar second harmonic generator was used to up-convert the IR pulses to 410 nm. The CW-equivalent power at 780 nm was 900 mW and at 410 nm it was 50 mW.

With a work function of 4.2 eV [10], ITO requires a 2-photon process is required at $\lambda =$ 410 nm (3.02 eV) for electron emission. At $\lambda = 780$ nm the photon energy drops to 1.59 eV

#255587 Received 14 Dec 2015; revised 12 Jan 2016; accepted 13 Jan 2016; published 16 Feb 2016

requiring three photons. For imaging at 780 nm the sample only exhibited interference patterns in the milled region most likely due to the residue left from the gallium milling. while the smooth un-milled region had no visible photoemission. The increased emission in the milled area is attributed to enhanced electric fields caused by surface roughness from the FIB process. The milled region at 780nm illumination only produced images for a short time period before the contrast disappeared. We suspect this to be due to surface smoothing and annealing in the intense illumination.

3. Experimental results

The area of interest is the central milled region seen in Figs. 1 and 2. The brightness in the image is proportional to the photoelectron yield, which relates to the electric field in the sample as

$$YPE \propto || E_{tot} ||^{2n}, \tag{1}$$

where n is the order of the photoemission process i.e. n = 2 for λ = 410 nm light and n = 3 for λ = 780 nm [5].

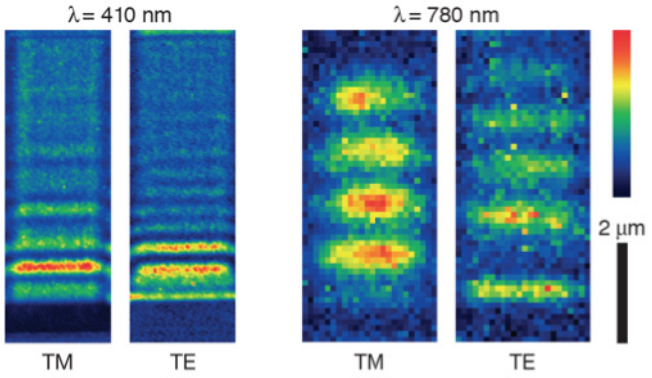

Fig. 2. Colorized PEEM images of the waveguide illuminated by TE and TM polarized light. Left and center left: two-photon PEEM (λ = 410 nm). Right and center right: three-photon PEEM (λ = 780 nm).

To obtain a Fourier transform of the interference patterns, we average the pixel value perpendicular to the propagation path and calculate the transform in the light propagation direction. The Fourier transform provides the spatial frequency spectrum of the interference pattern and is shown in Figs. 3 and 4.

The two main peaks in the periodograms represent the guided modes in the waveguide. These main modes are labelled 1 and 2. For the 410 nm illumination we observe two propagating modes in the 410 nm portions of the ITO, while the 780 nm illumination supports only one mode. In addition to the main modes of propagation several other peaks appear in the 410-nm periodograms. Interference between the two propagating modes, labeled 3, is visible with an interference spacing of just over 1 µm for TM polarization while it is lost in the noise for TE. Small peaks visible just above the noise level, labeled 4 are present as well.

These small peaks are the result of the non-linearity of the multiphoton emission process [5]. The photoemission yield in n-photon PEEM is proportional to the *n*th power of the sum of the different wave fields as in Eq. (1):

$$E_{total} = E_{incident} + E_{mode1} + E_{mode2}. \tag{2}$$

The cross terms produced by two- and three- photon emission introduce additional interferences, which appear in the Fourier analysis.

#255587 Received 14 Dec 2015; revised 12 Jan 2016; accepted 13 Jan 2016; published 16 Feb 2016

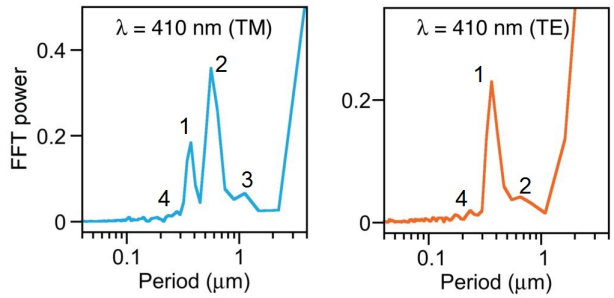

Fig. 3. Periodograms from the waveguide under 410-nm illumination. Left is TM and right is TE polarization. FFT powers in obtained by normalization to the photoemission yield obtained in the 410-nm TM case. (1, 2) Main propagating modes. (3) Interference of main modes. (4) multiphoton emission artifact peaks.

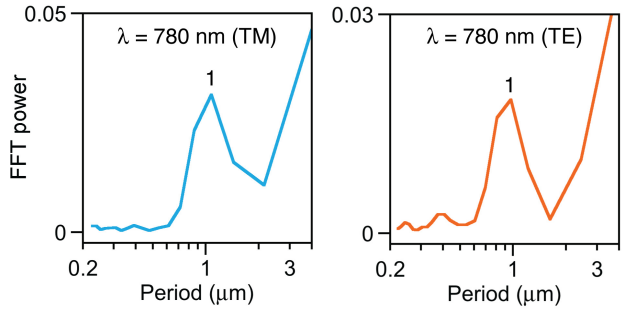

Fig. 4. Periodograms of the λ = 780 nm illuminated wave guide. The only significant peak is the single propagating mode.

4. Numerical model

The properties of dielectric waveguides have been well documented and the propagation of light can be numerically modeled by applying continuous boundary conditions for the electric field across the interface between the core and cladding [11]. We assume the propagation along the *z*-axis and write the time independent wave equation as:

$$\nabla^2 E(r) + k_0^2 n^2 E(r) = 0\,, \tag{3}$$

where n is the index of refraction, k_0 is the free space wave number and we assume that the time dependence is harmonic

Since our geometry is uniform along the y-axis dE/dy is zero. In the direction of propagation, the z-component, in the waveguide, the dependence is assumed to be exp(iβz). This reduces the wave equation in each layer of the wave guide to:

$$\frac{\partial^2 E}{\partial x^2} + \left(k_0^2 n_i^2 - \beta^2\right) E = 0\,, \tag{4}$$

where the index on n_i refers to the index of refraction of a particular layer. For TE polarization the only component of the electric field is E_y. By assuming evanescent fields in the cladding and substrate and requiring a continuous boundary condition across the interface one obtains an eigenvalue equation that depends on refractive indices, wavelength guide thickness and propagation constant. A complete formulation of this model can be found in optoelectronics texts such as [11]. The propagation constant provides the rate at which the phase travels along the guide:

$$\beta = k_0 n_i \sin\theta. \tag{5}$$

#255587 Received 14 Dec 2015; revised 12 Jan 2016; accepted 13 Jan 2016; published 16 Feb 2016

Since the pattern observed in PEEM is the interference of the incident and guided light one can extract the propagation parameters. It is customary to use the effective index that is related to the propagation constant by.

$$N_{eff} = \beta \frac{\lambda}{2\pi}. \tag{6}$$

To calculate the effective index of the dielectric structure a simple geometrical model is used. The separation of the interference pattern is used to determine the effective index, N_{eff}, of the waveguide assuming x is the distance the guided light travels before it is constructively interfered with by the incident light. $N_{eff} = \beta \frac{\lambda}{2\pi}$

$$\frac{x}{c / N_{eff}} = \frac{x \cdot \sin 60^{o} + \lambda}{c}; \tag{7}$$

$$N_{eff} = \sin 60^{o} + \frac{\lambda}{x}, \tag{8}$$

where λ is the wavelength and 60° is the angle of incidence We can thus determine the effective index of the waveguide from the experimentally observed interference pattern spacing determined from the periodogram.

5. Simulation

To simulate the PEEM results we use a 2-dimensional model in COMSOL as indicated in Fig. 5. COMSOL uses finite element methods to solve for the electromagnetic field on a mesh overlaying the geometry. For our purpose we produce an image of the time averaged real portion of the electric field.

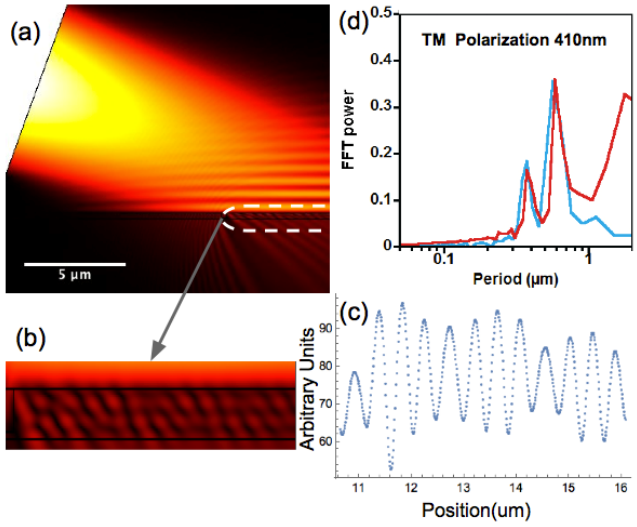

Fig. 5. (a) Time averaged electric field in finite element technique simulation using COMSOL multiphysics. (b) Close up of the guiding region supporting two modes. (c) Line graph of the electromagnetic field from the surface of the ITO layer. (d) Periodogram of simulated (red) and experimental (blue) TM polarization for λ = 410nm.

PEEM collects the electrons from the vacuum-ITO interface with the photo emission yield determined by the electric field strength Eqs. (1)-(2). Therefore we extract a line graph from the vacuum-air interface of the time averaged electric field intensity from the simulation. By taking the Fourier transform over the same distance as for the experimental we find good agreement between the simulation and experimental data for both polarizations and

#255587 Received 14 Dec 2015; revised 12 Jan 2016; accepted 13 Jan 2016; published 16 Feb 2016

wavelengths (Fig. 5). Furthermore the relative mode intensities (relative peak heights) of the two strongest modes of simulated data for λ = 410 nm correspond well to those of the experimental data. The discrepancy at long periods is due to the artifact produced by finite window size in the Fourier Transform. The position of this artifact differs between the experimental and simulated periodograms due to differences in windowing and data resolution. The relevant experimentally observed modes lie outside the range of the window-induced artifacts and can reliably be reproduced in the simulation.

6. The Goos-Hänchen effect

Commonly a ray optics representation is used to understand the propagation of light in a waveguide. The ray must travel at an angle within the waveguide such that a round trip of the ray across the guide obtains a phase that is an integer multiple of π. This is the transverse resonance condition is given by:

$$hk_0 n_1 \cdot \cos\theta - \phi_1 - \phi_2 = n\pi, \tag{9}$$

where n_1 is the index of refraction in the core of the wave guide and θ is the angle of propagation determined from the propagation constant in Eq. (5). The polarization dependent phase shifts, ϕ, are obtained at the reflection at the boundary and obtained from the Fresnel equations given by

$$\Phi_{TE} = \tan^{-1}\left[\frac{(n_{core}^2 \cdot \sin^2\theta - n_{cladding}^2)^{1/2}}{n_{core} \cdot \cos\theta}\right]; \tag{10}$$

$$\Phi_{TM} = \tan^{-}1\left[\frac{(n_{core}^2 \cdot \sin^2\theta - n_{cladding}^2)^{1/2}}{n_{core} \cdot \cos\theta} \cdot \frac{n_{core}^2}{n_{cladding}^2}\right]. \tag{11}$$

The subscripts TE and TM refer to transverse electric and transverse magnetic field polarizations. In this ray optics model the ray is confined completely inside of the waveguide undergoing total internal reflection at each interface as shown in Fig. 6(a).

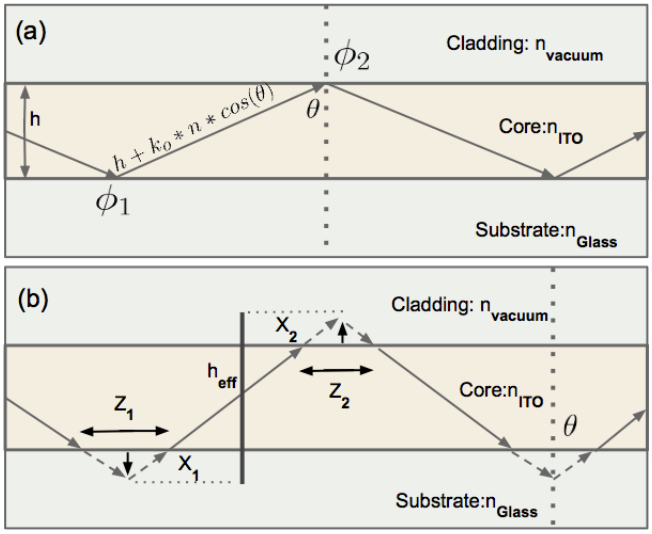

Fig. 6. (a) Ray model without the Goos-Hänchen shift with a round trip fulfilling the transverse resonance condition. (b) Ray model withthe Goos-Hänchen shift to account for penetration into the substrate.

This simple ray model does not allow for light to penetrate into the cladding and thus neglects the evanescent field. Including this light penetration in a ray model as in Fig. 6(b)

#255587 Received 14 Dec 2015; revised 12 Jan 2016; accepted 13 Jan 2016; published 16 Feb 2016

would seem more reasonable as first pointed out by Burke [12]. In this refined ray model the waveguide thickness is effectively increased by the depth the ray penetrates which is closely related to the characteristic decay length of the evanescent wave in the cladding [13].

This model has been shown to match with the electromagnetic theory [14] while keeping propagation along the lateral direction constant due to the time delay between the entering and exiting of the ray. The refined ray picture can be used as a reasonable model to understand the energy flow as well as power transfer in coupled wave guiding structures [15,16]. As seen in Fig. 6(b) the ray now under goes an apparent lateral shift that was first predicted by Newton [17] and has come to be known as the Goos-Hänchen shift after it was experimentally demonstrated by Goos and Hänchen in 1947 [7].

Calculation of the magnitude of the Goos-Hänchen shift was developed in 1948 by Artmann using a stationary phase method [18]. The formula can be derived by decomposing a finite beam into plane wave components. The phase upon reflection is angle dependent which is the root of the phenomena. The different phases obtained by each component produce the lateral displacement given as:

$$z_{TE} = 2\left(n_{core}^2 \cdot \sin^2\theta - n_{cladding}^2\right)^{-1/2} \tan\theta \frac{1}{k_0}; \tag{12}$$

$$z_{TM} = z_{TE}\left(\frac{n_{core}^2 \cdot \sin^2\theta}{n_{cladding}^2} + \sin^2\theta - 1\right)^{-1}. \tag{13}$$

These results give a good value for the shift but break down as the beam approaches to within half a degree of the critical angle. Other formulations have been proposed using approaches such as conservation of energy [19–21], but Artmann's formulation remains the simplest and provides an extremely good approximation for the shift. For our purposes the Artmann approach is sufficient.

Equations (12)-(13) are completely equivalent to the ray model which finds the shift through basic geometry:

$$z = 2x \cdot \tan\theta, \tag{14}$$

where x is the penetration depth into the substrate. This is closely related to the transverse decay constant by:

$$x = \frac{1}{\gamma q}; \tag{15}$$

$$\gamma = k_0\left(n_{core}^2 \cdot \sin^2\theta - n_{cladding}^2\right)^{1/2}, \tag{16}$$

where q is a polarization dependent factor based on the corresponding boundary conditions given by

$$q_{TE} = 1; \tag{17}$$

$$q_{TM} = \frac{n_{core}^2 \sin^2\theta}{n_{cladding}^2} + \sin^2\theta - 1. \tag{18}$$

We now compare the results obtained from the simulation, Artmann's formulas and the experimental data. To obtain a quantitative value for the Goos-Hänchen shift from the simulation we take the evanescent field decay from the time independent simulation as shown in Fig. 7. The decay depth is defined as the distance it takes for the field to decay to 1/e of its initial value [22]. This divided by the scale factor q from Eqs. (17)-(18) gives the penetration. The penetration depth then produces a shift through simple geometry of ray tracing as in Eq. (14) [23,24].

#255587 Received 14 Dec 2015; revised 12 Jan 2016; accepted 13 Jan 2016; published 16 Feb 2016

For comparison the Goos-Hänchen shift is directly calculated from Artmann's approach as expressed in Eqs. (12)-(13) using theoretical angles calculated from the known waveguide parameters and electromagnetic theory [11]. In the experimental case we obtain the effective indices for the propagating waveguide modes from the Fourier transform of the high-resolution PEEM images. By applying Eq. (8), with the known refractive indices of the materials, the angle of propagation θ can be calculated using Eqs. (5)-(6). This experimental θ provides the necessary information to calculate an experimental value for the Goos-Hänchen shift at the two interfaces using either detailed electromagnetic theory and ray penetration or good approximations such as Artmann. As the experiment lies within the validity range of Artmann's formulas, we use these to obtain the results.

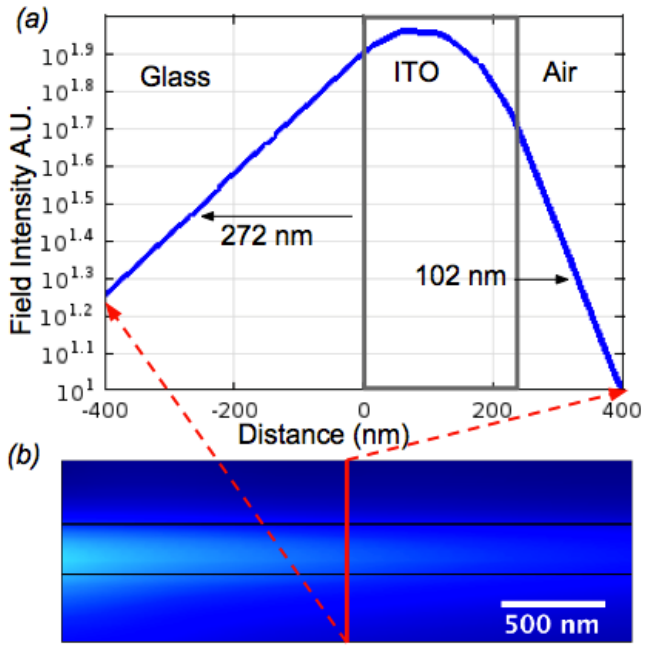

Fig. 7. (a) Semi-log line graph of electromagnetic field intensity taken across (b) a COMSOL simulated waveguide with h = 240nm, λ = 780nm, n_1 = 1.78, n_2 = 1.53, n_3 = 1. The graph is used to determine the penetration depth at each interface.

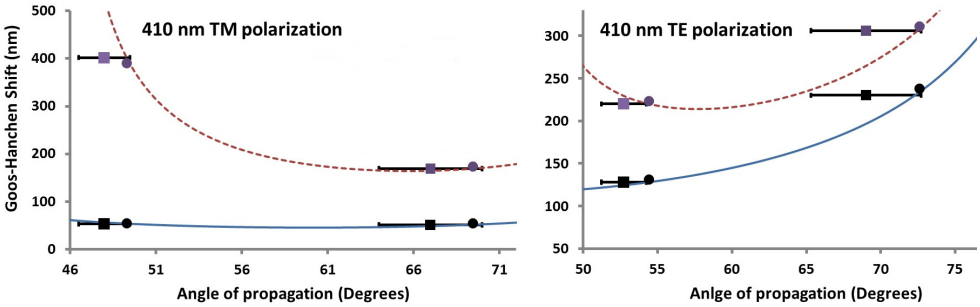

Fig. 8. Goos-Hänchen shift vs. angle of propagation at 410 nm for both interfaces and polarizations. Solid line (blue) is the theoretical shift at the air interface. Dashed line (red) is the theoretical shift at the glass interface. Squares represent experimentally determined data points at air interface (black) and glass interface (purple). Similarly circles are data points from simulation.

Results from theory, simulation and experiment are presented in Fig. 8. The simulated values are plotted at the theoretical angle and the shift as calculated from the ray method. The

#255587 Received 14 Dec 2015; revised 12 Jan 2016; accepted 13 Jan 2016; published 16 Feb 2016

experimental data is plotted at the theoretical shift with the angle as determined from the periodogram. The accuracy of mode 1 is considerably better than mode 2 as the shorter interfence spaceing provides more lines of interference along the length of the guiding structure. Simulated values agree to within 10 nm of the theoretical value. The slight variation can be attributed to the finite mesh and imperfect absorption at the boundaries of the model.

7. Conclusion

We have shown that interferometric microscopy in PEEM can provide a detailed picture of the wave propagation in thin films and at the interfaces of transparent media. The ability to provide resolution beyond the diffraction limit even in the non-linear regime of multi-photon excitations opens all of the optical range for this method and indicates that non-linear properties can also be probed.

Because of its small value, accurate experimental observation of the Goos-Hänchen effect has proved difficult. With the high resolution capabilities available in PEEM optical properties of small structures can be measured. Beyond basic science aspects there is currently increased interest in the measurement of Goos-Hanchen shifts. Small and even negative Goos-Hänchen shifts can be produced in materials with high imaginary index and in metamaterials [25]. Such negative shifts result in a reverse power flow in the cladding and this phenomenon can be exploited to trap or slow down light in the optical wavelength region [26,27]. These devices along with subwavelength dielectric resonators [28] can be easily modeled with the ray model when extended to include the Goos-Hänchen shift.

Acknowledgments.

This research was supported by the Basic Science Office of the Department of Energy under grant no. DE-FG02-07ER46406

The authors gratefully acknowledge useful discussions with Dr. J. P. S. Fitzgerald.

#255587 Received 14 Dec 2015; revised 12 Jan 2016; accepted 13 Jan 2016; published 16 Feb 2016